

# Identifying faults and fractures using source mechanism inversion, *b* values, and energy release rates

Abstract:

Identifying and differentiating between fracture stimulation and fault activation is critical to achieving successful and efficient hydraulic treatment in unconventional reservoirs. Source mechanism inversion of the first P-wave arrivals detected by a large aperture near surface array indicates how the formation fails under imposed stress. Creating a frequency magnitude distribution histogram and graphing energy released through time for each observed mechanism can be used to correlate event populations with fault motion or fracture propagation. We use source mechanism inversion to identify two unique event populations for which we calculated *b* values and energy release rates. We interpreted one population to be associated with fault re-activation and the second with natural fracture stimulation.

Introduction:

Microseismic monitoring in low permeability reservoirs is a valuable source of information for unconventional resource play optimization. The application of new technologies, such as efficient horizontal drilling and hydraulic fracturing (“fracking”) has resulted in the ability for the industry to produce from organic rich shales. Prior to such technology developments, hydrocarbons from such formations were typically not economically accessible or even recoverable. Monitoring of microseismicity is essential to understanding how a formation responds to the injection of frac fluids and proppant because many of the most active shale plays remain in the early stages of development and a wide range of geologic hazards may be present, such as faults, karst collapse features, and proximal aquifers. Microseismic monitoring provides the necessary information to estimate stimulated reservoir volume (SRV) and identify faults that are unresolvable with reflection seismic data that may pose a hazard to completion operations.

A successful frac will typically increase the permeability of fine grained hydrocarbon reservoirs—thus enhancing the well’s production and delivering a significant rate of return. This is achieved by stimulating an existing network of natural fractures (Maxwell et al., 2006; Gale et al., 2007). Hydraulically stimulated natural fractures are generally near the wellbore and are a primary receiver of proppant necessary to create a flow pathway to the wellbore. In some cases, a horizontal wellbore will encounter a pre-existing stressed tectonic fault. Pumping of fluids and

proppant into a fault can bring about one or more unintended negative effects. A non-target formation may be stimulated and give rise to hydraulic connectivity with aquifers that ultimately increase water production. Another risk is diversion of fluid and proppant to a fault zone that lies several hundred feet away from the target fracture stage. The end result is decreased stimulation of the target formation, a potential increase in water production, and a significant cost to the operator in terms of time and materials. Having the ability to differentiate between faults and fractures in a timely manner is critical to reducing such material waste which could be otherwise employed in areas that are more favorable for effective stimulation.

Understanding the source mechanism of a microseismic event leads to improved event location and provides information vital to generating realistic reservoir models. Source mechanisms indicate how the formation fails under stress; the polarity of the first P-wave arrival indicates relative motion along the failure plane. Identification of one or more source mechanisms within microseismic data recorded during hydraulic fracturing provides information about the current stress state of the formation and, where multiple source mechanisms exist, can also be used to differentiate between reactivation of a stressed tectonic fault and desirable natural fracture stimulation.

Statistical analysis using frequency magnitude distribution histograms (FMD) may be indicative of changes in the stress magnitude (Schorlemmer et al., 2005; Gulia et al., 2010), and in the following case study, determines if a population of events is generated by fault motion or natural fractures. The FMD relationship was first identified by Gutenberg and Richter (1954) and demonstrated in the formula:

$$\log N = A - bM_s$$

where *N* is the number of events with magnitudes within a fixed interval around *M<sub>s</sub>*. *A* and *b* are constants. The constant *b* for a specific event population represents the frequency of occurrence for different size events; a higher slope indicates fewer large events and more small events than a lower slope *b* value. Maxwell et al. (2009) and Downie et al. (2010) observed during a hydraulic treatment that fault related microseismicity is correlated to *b* values of ~1 while desirable induced natural fracture related microseismicity exhibits a *b* value of ~2.

Downie et al. (2010) recognized that microseismicity that occurred after treatment ceased was located along a known fault. Another way of stating this concept is that microseismicity generated by activation of natural fractures during hydraulic stimulation is mechanically dependent upon pumping whereas fault activity is not. Therefore

natural fracture events will take place during pumping, and fault activation events will take place during a much longer period of time. This is due to the higher stress imposed on the fault that is slowly released with an overall lower  $b$  value.

#### Methods:

Microseismic data was acquired using a BuriedArray™ permanent near surface passive seismic array (Figure 1). There are 206 surface locations distributed across an area of approximately 144 square kilometers. Each surface location has three vertical component geophone channels at depths of 100-200 feet. Acquired data was transmitted from each station to a Wi-Fi receiving tower with a sample rate of 2 ms. Once acquired, all of the individual traces are merged and preprocessed with a bandpass filter and a proprietary spectral whitening filter. The data is then processed using Passive Seismic Emission Tomography (PSET®) technology. The PSET® algorithm is used to determine the location of microseismicity generation and also to match the microseismic event to one of several possible source mechanisms. The detected events are shown in Figure 2.

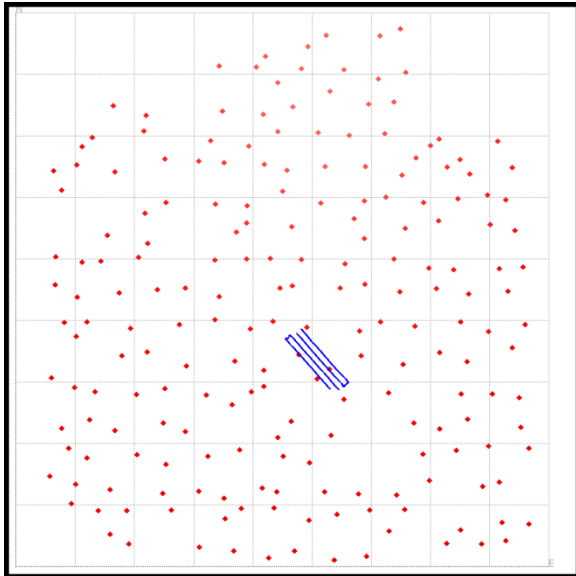


**Figure 1.** Map of BuriedArray™ stations and location of wells used in this case study. Each red dot represents a wellbore location in which 3 vertical component stations are buried 100-200 feet deep. Grid spacing is 5000' x 5000'.

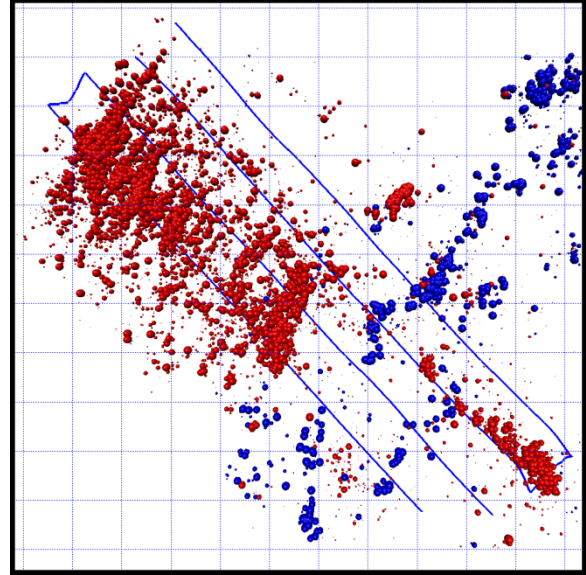


**Figure 2.** Map view of all events detected during treatment. The first several stages of each well were not monitored. Events are sized by moment magnitude and colored by focal mechanism. Red events are oblique dip-slip with dip/strike/rake of 40°/90°/-125°. Blue events are strike-slip along a failure plane of 240°/80°/10°. Grid squares are 500' x 500'.

Source mechanism inversion is performed using a least squares inversion of observed P-wave amplitudes and polarities from the vertical component geophones (Williams-Stroud et al., 2010). While it is possible to use both P- and S-waves observed at the surface to invert the moment tensor, the wide aperture and azimuthal coverage provided by the near surface array ensures a robust solution without the need for S-wave amplitudes. The inversion algorithm is capable of solving for full moment (including a volumetric portion) and double-couple (shear) mechanisms with a high level of accuracy while negating limitations imposed by array geometry. The moment tensor is inverted from a point source relationship between observed vertical component displacements  $A$  and moment tensor components  $M_{jk}$ :

$$A = G_{3,j,k} M_{jk}, \quad (1)$$

with  $G_{3,j,k}$  representing the vertical components of the Green's function derivative. Einstein's summation rules apply (Aki and Richard, 1980). Inversions using equation (1) may be performed using least squares (Sipkin, 1982) or a grid search. A grid search can only be used to identify pure shear sources because a non-shear source would have an infinite number of possible  $M_{jk}$  combinations. Assuming a homogeneous isotropic medium, the Green's function derivative corrected for attenuation is written:

$$G_{3j,k} = \frac{M_0}{4\pi\rho rc^3} \gamma_3 \gamma_j \gamma_k e^{\frac{\pi r f}{cQ}}. \quad (2)$$

Although natural systems are inherently heterogeneous, the wide aperture array compensates for model heterogeneity and still provides accurate estimates of fault plane orientation (Šílený, 2009). Further information regarding source mechanism inversion can be found in Williams-Stroud et al. (2010). The source mechanisms used in this study represent inversions that best fit the observed spatial trends of microseismic events.

Slope values (*b* values) are established using the maximum likelihood method put forth by Woessner and Weimer (2005). FMDs are determined by first separating events into 0.1 moment magnitude bins and plotting the log of the bin count against the moment magnitude of the bin. The *b* value is the slope of the histogram for events greater than the magnitude of completeness. The magnitude of completeness,  $M_c$ —the smallest magnitude at which all events of that size are detectable—is calculated using maximum curvature method (Woessner and Weimer, 2005) and is -1.6 for this study. Spatial *b* value analysis is implemented using Zmap software (Weimer, 2001) which operates in MATLAB. Grid cells of 0.001 degrees latitude and longitude are used to create maps of *b* values across the area of interest.

Microseismic events are converted from moment magnitude to Joules of energy released using the following formula:

$$\log J = 1.5M_w + 4.8 \quad (3)$$

where *J* is the energy released in Joules and  $M_w$  represents the moment magnitude. This equation is derived from that used by Kanamori and Anderson (1975) to convert moment magnitude to ergs and follows the Gutenberg-Richter energy relationship (Gutenberg and Richter, 1956). The cumulative microseismic energy for a selected 24 hour period is summed and normalized to 1 for each mechanism to eliminate biases from differing event counts and total cumulative energy released. Slopes are calculated within chosen time windows to demonstrate the variability of energy release per unit time for each mechanism.

Case Study:

The target formation of this study is the Lower Barnett Shale of the Ft. Worth basin in the Mid-Continent U.S. The formation lies unconformably over the Viola/Simpson and Ellenberger Limestones. The monitoring array is

located adjacent to the Muenster Arch in North Texas. Maximum horizontal stress in this area is estimated to be approximately NE-SW (Heidbach et al., 2009) and reactivated fractures are expected to propagate in this direction. Natural fractures dip steeply (>75°), are oriented WNW-ESE (Waters et al., 2006, Gale et al., 2007), and are commonly healed with calcite (Waters et al., 2006; Bowker, 2007). Gale et al. (2007) suggests that fracture density is variable, with clusters of large fractures spaced several hundred feet apart. Source mechanism analysis was unable to identify a source mechanism aligned with the orientation of these natural fractures and therefore they do not contribute significantly to the observed microseismicity. The orientation of maximum stress oblique to existing natural fractures creates a scenario well suited to the creation of a complex fracture network.

Two distinct source mechanisms were identified in the observed treatment (Figure 3). The dominant mechanism associated with natural fracture stimulation has a strike of 40°, a dip of 90°, and a rake of -125° (40°/90°/-125°). This oblique dip-slip failure plane is present throughout the treatment area. The events with this mechanism are generally within 1,000' of the wellbore and are associated with opening of natural fractures in the formation. The second mechanism is a nearly vertical strike-slip failure plane oriented 240°/80°/10°. Events of this mechanism form a linear trend approximately 6,000' in length oriented SW-NE. The linear spatial trend and the strike-slip motion on the failure plane suggests that this is an existing stressed tectonic fault. The difference in slip motion between the two source mechanisms in such close proximity indicates low stress anisotropy; maximum and minimum horizontal stresses are very similar. Although the two mechanisms have similar strike directions, PSET® is capable of identifying the source mechanism of each event and the consistency of the spatial trends confirms this.

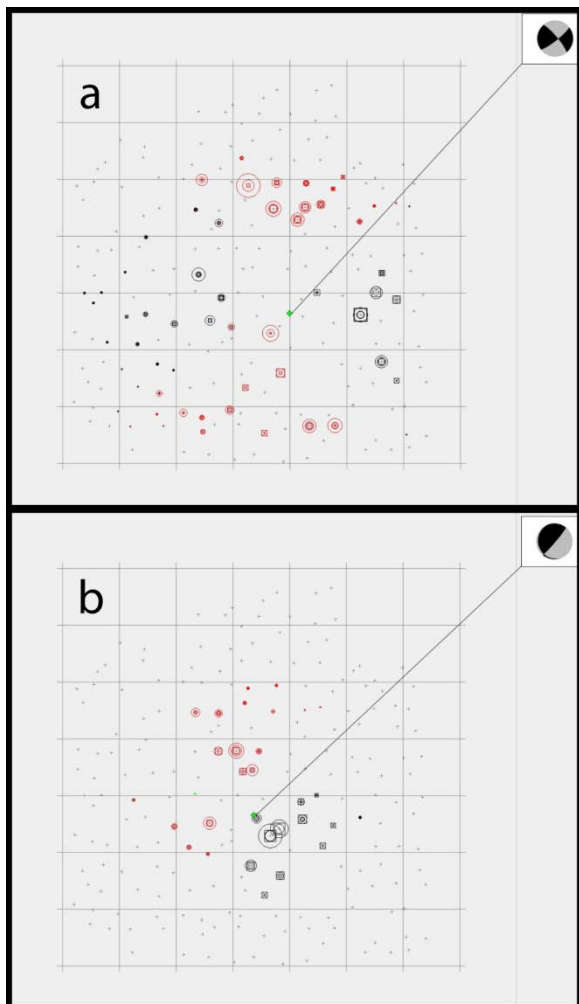


**Figure 3.** Map of first arrivals to buried geophones. Each dot represents a station. Red indicates a negative first arrival and upward motion whereas black is positive polarity and downward motion. (a) Strike-slip fault activation source mechanism. (b) Dip-slip fracture stimulation source mechanism.

After dividing the microseismic events into two populations based on source mechanism, a frequency magnitude distribution analysis (Figure 4) indicates whether a mechanism is associated with stimulation of natural fractures or a stressed tectonic fault. The slope of the FMD histogram indicates that the dip-slip events have a  $b$  value of  $\sim 2.2$  and the strike-slip events have a slope of  $\sim 1$ . These values verify that dip-slip events are generated by natural fracture stimulation while strike-slip events are generated by motion along a fault plane. Spatial  $b$  value analysis reveals that areas dominated by the dip-slip failure correspond to higher  $b$  values while lower  $b$  values are concentrated in the linear zone oriented SW-NE associated with strike-slip fault motion (Figure 5). The  $b$  values near the perimeter of the colored zone are anomalously high as a result of insufficient sample populations within a cell. Cell by cell  $b$  values in fault and frac zones are comparable and

in agreement with  $b$  values calculated for their respective event populations (Figure 6). The Zmap generated map of  $b$  values on a cellular grid also confirms that distinction between fault and fracture can be derived from source mechanism inversion.

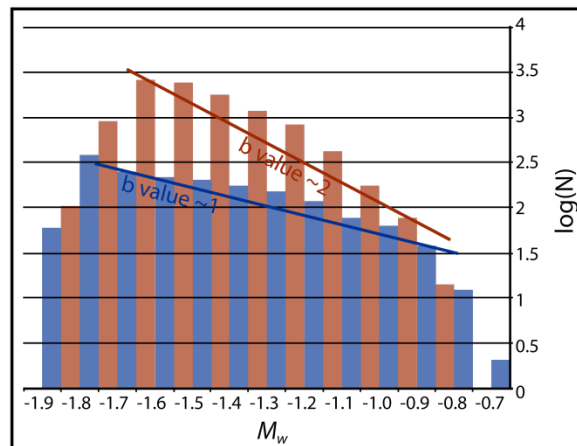


**Figure 4.** Non-cumulative FMD histograms of fracture stimulation events (red) and fault activation events (blue) showing the log of the number of events (y-axis) per 0.1 moment magnitude bin (x-axis). Fracture stimulation events have a  $b$  value of  $\sim 2$  whereas the fault activation event  $b$  values are  $\sim 1$ .

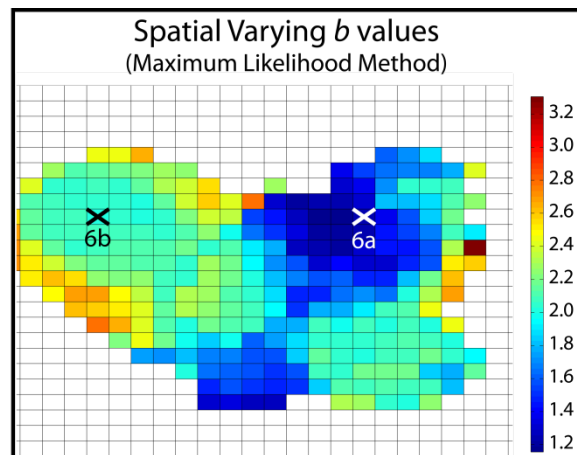


**Figure 5.** Map of  $b$  values within treatment area displayed on a cellular grid. Where  $b$  values are  $\sim 2$  (light blue to green) treatment stimulated predominantly natural fractures. Dark blue colors indicate lower  $b$  values and significant fault activation. The highest values at the perimeter are due to an insufficient sample size within the cell. Cells used in Figure 6 are indicated.

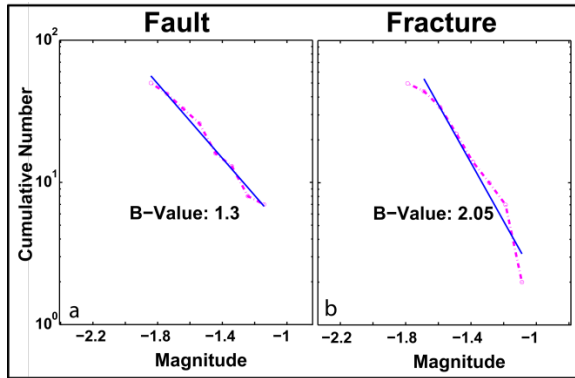


**Figure 6.** Cumulative FMD plots for individual cells indicated in Figure 4. (a) The lower  $b$  value of 1.3 indicates that the cell is dominated by fault activity. (b) The fracture cell  $b$  value of 2.05 indicates greater fracture stimulation.

A 24 hour period of activity that included significant fault activity and fracture stimulation was selected for energy release rate analysis (Figure 7). Three individual fracture treatment stages took place during this 24 hour period (Figure 8). The first stage was adjacent to the fault and released energy was focused along the fault zone with strike-slip source mechanism events. Strike-slip events continued to occur along the fault zone for the remainder of the 24 hour time interval. The two subsequent treatment stages were located an adequate distance away from the fault to avoid diversion of pumped fluid and proppant into the fault zone. The recorded microseismicity was comprised almost entirely of events with a dip-slip source mechanism and a only minor amount of strike-slip events continuing from stimulation of the fault during the previous stage. The resulting energy release rates (Table 1, slope 1b, 2b) are initially high and reduce gradually until the treatment is complete, at which time the energy release rate is very low. The dip-slip mechanism events are isolated to pumping time and are therefore mechanically dependent while strike-slip mechanism events are distributed throughout the 24 hour period, including time between pumping, and are therefore mechanically independent. This further substantiates the effectiveness of separating event populations by source mechanism to differentiate between fracture stimulation and fault activation.

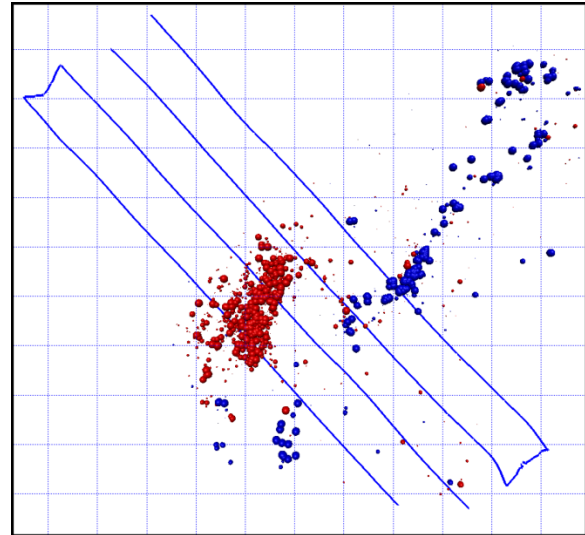


**Figure 7.** Map of microseismicity generated during a 24 hour period. Events are sized by moment magnitude and colored by source mechanism. Red events are dip-slip associated with fracture stimulation and blue events are strike-slip related with fault activation. Grid squares are 500' x 500'.

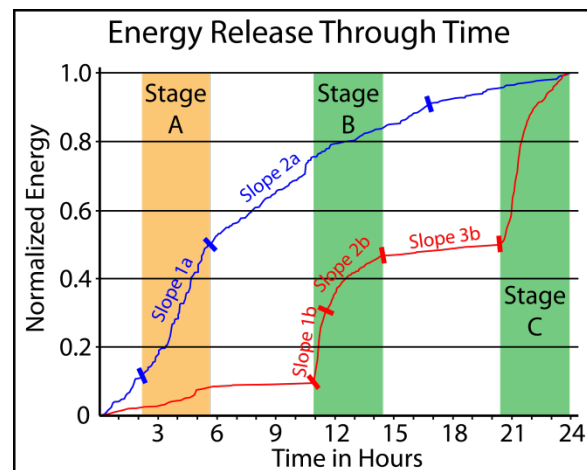


**Figure 8.** Normalized cumulative energy released during the selected 24 hour period. Pumping during stage A created a large amount of fault related microseismicity and very little fracture stimulation. Later stages (B and C) were effective at stimulating natural fractures.

**Table 1. Slope Values**

Failure Type	Slope	Slope Value (J/s)
Fault	1a	9.0
	2a	3.0
Fracture	1b	42.2
	2b	7.8
	3b	0.8

#### Discussion:

According to Schorlemmer et al. (2005) and Gulia et al. (2010), higher stress regimes correlate with lower  $b$  values. When applying this concept to the data presented within this study, we can make the inference that lower  $b$  values

are associated with long linear trends of microseismicity. Higher  $b$  values indicate greater fracture complexity due to the increased number of smaller events, and therefore a more effective stimulation. Following the work of Maxwell et al. (2009) and Downie et al. (2010), we are able to validate the difference in  $b$  value between fault activation and fracture stimulation. Greater precision in distinguishing faults and fractures is possible by using source mechanism inversion to segregate the data in lieu of only using the pumping time. Making this distinction with source mechanisms is necessary for identifying fault activity during pumping and confirming that fracture stimulation is mechanically dependent upon pumping. It also allows more accurate calculation of  $b$  values and energy release rates. A surface or near surface array is well suited to this task because it has a wide azimuth and large aperture which allows accurate source mechanism inversion—something that a single downhole array is unable to provide.

By combining source mechanism inversion with  $b$  values and energy release rates, operators can identify areas of effective stimulation and minimize waste of fluids, proppant, and time. For example, in this study we are able to identify understimulated areas of the reservoir adjacent to the fault trend. Considering this information while calculating the stimulated reservoir volume will provide a more accurate estimate of the volume of stimulated rock if fault related events are either excluded or accounted for but with a reduced level of influence. Early identification of fault trends during real time microseismic monitoring can reduce stimulation of non-target formations that may potentially lead to hydraulic connectivity with aquifers that in turn result in increased water production. Once a fault is identified, a plan can be implemented to resume hydraulic treatment a safe distance away to prevent further stimulating the fault zone which would substantially reduce return on investment.

Identifying multiple source mechanisms is the only way to effectively discriminate between fault activation and fracture stimulation, regardless of whether pumping is ongoing or not. Areas with existing stressed tectonic faults are likely to exhibit multiple source mechanisms representing both fracture stimulation and fault activation. Calculation of  $b$  values requires a relatively large population of events to arrive at a robust solution; however this is rarely an issue. Abnormally high  $b$  values are indicative of an inadequate microseismic event population.

Future research should be carried out in a similar manner with other wells that intersect stressed tectonic faults in a different target formation. Integration of 3D seismic attributes with the cellular map of  $b$  values could provide more insight into stimulation efficiency.

#### Conclusions:

Source mechanism inversion is necessary to discriminate between fault activation and fracture stimulation and can only be acquired with wide azimuth surface or near surface array or a minimum of two typical downhole observation wells.. It enables identification of events that are fault or fracture related regardless of the time of the event with more accurate  $b$  values and energy release rates. Stimulated reservoir volumes can be more accurately estimated by accounting for microseismicity associated with unfavorable fault activity and comparing with a spatial grid of  $b$  values to identify areas that experienced more or less effective stimulation. Areas with higher  $b$  values may indicate greater stimulation complexity. By integrating source mechanism inversion with these two techniques we can identify faults and fractures more confidently, especially when they are spatially coincident.

#### Acknowledgments:

#### References:

- Aki and Richards, 1980: Quantitative seismology. Theory and Methods. Freeman, San Francisco, Calif.
- Bowker, K.A. 2007, Barnett Shale gas production, Fort Worth Basin: Issues and discussion. AAPG Bulletin V. 91. No. 4, p. 523-533.
- Downie, R.C., Kronenberger, E., Maxwell, S.C. 2010. Using Microseismic Source Parameters to Evaluate the Influence of Faults on Fracture Treatments - A Geophysical Approach to Interpretation," SPE 134772 presented at the Society of Petroleum Engineers, Florence, Italy, September 19-22.
- Gale, J. F., Reed, R. M., and Holder, Jon, 2007, Natural fractures in the Barnett Shale and their importance for hydraulic fracture treatments, AAPG Bulletin, 91, no. 4, p. 603 – 622.
- Gulia, L., Wiemer, S., & D. Schorlemmer, 2011, Asperity-based earthquake likelihood models for Italy. Annals of Geophysics, 53.3 (2010): p. 63-75.
- B. Gutenberg and C.F. Richter, Seismicity of the Earth and Associated Phenomena, 2nd ed. Princeton, N.J.: Princeton University Press, 1954.
- Gutenberg, B., and C. F. Richter, 1956, Magnitude and energy of earthquakes, Ann. Geofis., 9,p. 1-15.
- Heidbach, O., Tingay, M., Barth, A., Reinecker, J., Kurfeß, D., Müller, B., 2009, The World Stress Map based on the database release 2008, equatorial scale 1:46,000,000, Commission for the Geological Map of the World, Paris, doi:10.1594/GFZ.WSM.Map2009.

- Kanamori, H., and D. L. Anderson, 1975, Theoretical basis of some empirical relations in seismology, *Bull. Seismol. Soc. Amer.*, 65, p. 1073-1096.
- Maxwell, S.C., Waltman, C.K., Warpinski, N.R., Mayerhofer, M.J., and Boroumand, N., 2006, Imaging seismic deformation induced by hydraulic fracture complexity, SPE102801, Society of Petroleum Engineers.
- Maxwell, S.C., Jones, M., Parker, R., Miong, S., Leaney, S., Dorval, D., D'Amico, D., Logel, J., Anderson, E., Hammermaster, K., 2009. Fault Activation During Hydraulic Fracturing, SEG Expanded Abstracts 28, 1552.
- Schorlemmer, D., Wiemer, S., and M. Wyss, 2005, Variations in earthquake-size distribution across different stress regimes, *Nature*, vol. 437, p. 539-542.
- Šílený, J., Hill, D. P., Eisner, L. and Cornet, F. H., 2009, Non-doublecouple mechanisms of microearthquakes induced by hydraulic fracturing. *J. Geophys. Res.*, 114, B08307.
- Sipkin, S.A., 1982, Estimation of earthquake source parameters by the inversion of waveform data: synthetic waveforms, *Phys. Earth planet. Inter.*, 30, p. 242-259.
- Waters, G., J. Heinze, R. Jackson, A. Ketter, J. Daniels, and D. Bentley, 2006, Use of Horizontal Well Image Tools to Optimize Barnett Shale Reservoir Exploitation: SPE 103202, presented at the SPE Annual Technical Conference. DOI: 10.2118/103202-MS.
- Wiemer, S., 2001, A software package to analyze seismicity: ZMAP, *Seismological Research Letters*, 72, p. 374– 383.
- S. Williams-Stroud, L. Eisner, A. Hill, P. Duncan & M. Thornton. 2010. Beyond the Dots in the Box – Microseismicity-constrained Fracture Models for Reservoir Simulation presented at EAGE Barcelona, Spain 2010.
- Woessner, J., and S. Weimer, 2005, Assessing the quality of earthquake catalogs: Estimating the magnitude of completeness and its uncertainty, *Bulletin of the Seismological Society of America*, vol. 95 no. 2, p. 684-698.